

Carbon-detected deuterium solid-state NMR rotating frame relaxation measurements for protein methyl groups under magic angle spinning

Liliya Vugmeyster^{a,*}, Dmitry Ostrovsky^b, Riqiang Fu^c

^a Department of Chemistry, University of Colorado Denver, Denver, CO, 80204, USA

^b Department of Mathematics, University of Colorado Denver, Denver, CO, 80204, USA

^c National High Field Magnetic Laboratory, Tallahassee, FL, 32310, USA

ARTICLE INFO

Keywords:

Solid-state NMR
Deuterium
Cross-polarization
Rotating frame relaxation
Magic-angle spinning
Protein dynamics

ABSTRACT

Deuterium rotating frame solid-state NMR relaxation measurements (${}^2\text{H } R_{1\rho}$) are important tools in quantitative studies of molecular dynamics. We demonstrate how ${}^2\text{H}$ to ${}^{13}\text{C}$ cross-polarization (CP) approaches under 10–40 kHz magic angle spinning rates can be combined with the ${}^2\text{H } R_{1\rho}$ blocks to allow for extension of deuterium rotating frame relaxation studies to methyl groups in biomolecules. This extension permits detection on the ${}^{13}\text{C}$ nuclei and, hence, for the achievement of site-specific resolution. The measurements are demonstrated using a nine-residue low complexity peptide with the sequence GGKGMGFGL, in which a single selective $-{}^{13}\text{CD}_3$ label is placed at the methionine residue. Carbon-detected measurements are compared with the deuterium direct-detection results, which allows for fine-tuning of experimental approaches. In particular, we show how the adiabatic respiration CP scheme and the double adiabatic sweep on the ${}^2\text{H}$ and ${}^{13}\text{C}$ channels can be combined with the ${}^2\text{H } R_{1\rho}$ relaxation rates measurement. Off-resonance ${}^2\text{H } R_{1\rho}$ measurements are investigated in addition to the on-resonance condition, as they extend the range of effective spin-locking field.

1. Introduction

Deuterium solid-state NMR rotating frame relaxation measurements serve as an important tool in quantitative studies of molecular dynamics in a variety of systems from materials to complex biological molecules [1–9]. Recent advances focused on applications of deuterium NMR to multiply-labeled biomolecules, which require acquisition under magic-angle spinning (MAS) and transfers of polarization to nuclei with a large chemical shift dispersion, such as carbon-13, to obtain site-specific resolutions [1,2,10–13]. Internal motions in biomolecules on μs – ms time scale range are essential for a variety of biological functions [14–16], and rotating frame relaxation is one of the major tools to provide information for these times scales [17–20].

1.1. The goals of the work: inclusion of the ${}^2\text{H}$ – ${}^{13}\text{C}$ CP block to the ${}^2\text{H } R_{1\rho}$ measurements

We have recently demonstrated the utility of deuterium rotating frame NMR measurements for dynamics investigations in a variety of powder samples from model compounds to short peptides, to amyloid- β fibrils, under static and magic angle spinning (MAS) conditions [9,

21–23]. In these applications a single chemically distinct site was labeled with deuterium. The goal of this work is to demonstrate how the ${}^2\text{H } R_{1\rho}$ experiments can be combined with the ${}^2\text{H}$ to ${}^{13}\text{C}$ polarization transfer to retain the inherent deuterium rotating frame relaxation rates yet render effective polarization transfer for the detection on the ${}^{13}\text{C}$ nuclei. In particular, we aim to demonstrate feasibility of these measurements for mobile protein methyl groups.

Deuterium is a quadrupolar nuclei and has a spin of 1. The quadrupolar coupling constant is about 160–200 kHz for the full-width quadrupolar tensor and 53–60 kHz for methyl groups undergoing fast rotation about the threefold axis [1,5,24]. This large-magnitude coupling constant can be compared with the much small ${}^2\text{H}$ – ${}^{13}\text{C}$ dipolar coupling constant on the order of 3.5 kHz. Thus, the polarization transfer steps between ${}^2\text{H}$ and spin ${}^{13}\text{C}$ nuclei are not as straightforward as more traditional proton to spin $1/2$ nuclei transfers [11,25,26]. The optimization of the transfer is usually focused on maximizing signal intensity and covering the maximum range of quadrupolar frequencies present in the powder sample. For methyl groups the situation is somewhat relaxed due to the smaller effective value of the quadrupolar coupling constant. Polarization transfers between deuterons and spin- $1/2$ nuclei using the adiabatic RESPIRATION cross-polarization

* Corresponding author. Department of Chemistry, University of Colorado at Denver, 1201 Larimer St, Denver, CO, 80204, USA.

E-mail address: LILIYA.VUGMEYSTER@UCDENVER.EDU (L. Vugmeyster).

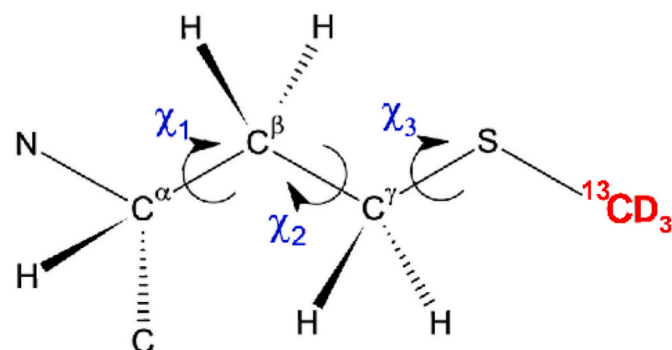
(AD-Resp-CP) has been proposed as one of the most effective methods at low and moderate MAS rates [27]. This scheme utilizes a relatively low power on the deuterium channel. Other approaches are based on employment of linear ramps or adiabatic sweeps for the cross-polarization steps to expand the covered range of quadrupolar frequencies present in the solid state [10,25,28,29]. The optimal control method has been employed as another alternative [30].

We focus on the implementation of the polarization transfer step between ^2H and ^{13}C nuclei into the $^2\text{H} R_{1\rho}$ experiments for two methods: the adiabatic sweep CP (ADCP) and AD-Resp-CP with the MAS rates in 10–40 kHz. As will be elaborated in the results section, the functional form of the RF amplitude modulation is in many ways similar in these two schemes. The results are shown for both on-resonance and off-resonance cases, the latter with the employment of the additional adiabatic ramps to align the deuterium magnetization along the tilted frame. We demonstrate experimental considerations that ensure that the polarization transfer steps do not skew the observed relaxation rates. This is achieved by comparing the $^2\text{H} T_{1\rho} = 1/R_{1\rho}$ times to those obtained with direct deuterium detection. The best results are obtained when the deuterium spin-lock RF amplitude matches the initial RF amplitude during the ADCP adiabatic sweep ramp or the RF amplitude of the short series of the pulses on the ^2H channel for the AD-Resp-CP scheme.

1.2. Overview of the model system: a nine-residue peptide with the low complexity sequence and with a singly labeled methyl group

We utilize a synthetic nine-residue peptide with the primary sequence of GGKGMGFGL, which has ^{13}C and ^2H labels incorporated at the M5 methyl group (Fig. 1). The sequence exhibits the so-called “low complexity” pattern, displaying the disordered state of the backbone. Prior assignments in solution as well as circular dichroism measurements confirmed the disordered structure [31,32]. The M5 methyl group assignment in the solid state was obtained from the ^1H to ^{13}C CP one-dimensional spectrum and indicated that the chemical shifts of this methyl group are close in the solution and solid state (Fig. S1) [32]. In turn, this points to similar rotameric populations around the χ_3 dihedral angle [33].

We have previously investigated in detail rotameric interconversions of the mobile M5 side-chain using ^2H NMR $R_{1\rho}$ measurements in the solid state under static conditions, while employing the version of the peptide labeled only with deuterium [32]. The peptide employed in this work, with the $^{-13}\text{CD}_3$ label at the M5 position, serves as an excellent model to test the extension of the $^2\text{H} R_{1\rho}$ NMR relaxation



GGKGMGFGL

Fig. 1. The labeling pattern of the M5- $^{13}\text{CD}_3$ side-chain of the RC9 peptide with the sequence GGKGMGFGL. Also displayed are the three side-chain dihedral angles, around which the rotameric interconversions are possible.

method to ^{13}C -labeled proteins. The rest of the peptide does not have ^{13}C labeling, thus the method development can be conveniently carried out in the one-dimensional fashion.

2. Materials and methods

2.1. Peptide preparation

The methionine- $^{13}\text{CD}_3$ amino acid was purchased from Cambridge Isotope laboratories. The 9-Fluorenylmethyl chloroformate (Fmoc) group was added to the Met- $^{13}\text{CD}_3$ amino-acid by Life Technologies Inc, and the purity and identity of the compound has been verified by mass-spectroscopy, high pressure liquid chromatography (HPLC), and solution ^1H and ^{13}C NMR spectra of the resulting modified amino acid. The RC9 peptide with the sequence GGKGMGFGL was then prepared using solid-state peptide synthesis with the Fmoc-based chemistry by Life Technologies, Inc. and purified by reversed-phase HPLC using the C18 column and water/acetonitrile buffer system with trifluoroacetic acid as the co-factor. The purity of the peptide at the 97% level was confirmed by analytical HPLC and matrix-assisted laser desorption/ionization mass spectroscopy, as well as proton solution NMR. 2 mg of dry lyophilized peptide was packed into a 1.3 mm rotor for the solid-state studies under MAS.

2.2. NMR spectroscopy

The measurements under MAS conditions were performed using the 14.1 T spectrometer at the National High Magnetic Field Laboratory (Tallahassee, FL), utilizing the Bruker 1.3 mm HXY probe tuned to the HCD configuration. The maximum achievable power on the ^2H channel is 75 kHz for the 90° excitation pulses, as calibrated using the methyl group of M5-RC9 sample, which has the motionally averaged quadrupolar coupling constant of 30 kHz [32]. The ^{13}C chemical shift was referenced using the gamma polymorph of glycine [34]. For carbon-detected spectra 1024 complex points were collected with the spectral width of 100 kHz. For the ^2H -detected spectra 2048 to 4096 complex points were collected with the spectral width of 250 kHz. The hard power excitation 90° pulses were 3.3 μs on the deuterium channel. In the $^2\text{H} R_{1\rho}$ measurements the inter-scan delays of 1.5–2 s were used. 8 dummy scans were used and the number of acquisition scans varied between 48 and 128 for the ^2H direct detection measurements and between 384 and 768 for the ^{13}C detected measurements. 10 to 12 relaxation delays were collected to obtain the magnetization decay profiles. Other experimental details of the CP schemes, the $^2\text{H} R_{1\rho}$ measurements, and ^2H longitudinal relaxation times measurements are elaborated in the Results section. The temperatures stated represent the set points, without further adjustments.

The ^{13}C longitudinal relaxation time at 40 kHz MAS and 280 K was determined using the one-dimensional saturation recovery measurements with 8 relaxation delays in 0.5–30 s range and 8 scans, using ^{13}C 90° pulses of 5.5 μs for the one-pulse detection scheme. The rotor-synchronized Hahn-echo based proton decoupling [35] at 80 kHz power was utilized during the acquisition.

3. Results

3.1. Establishing ^2H to ^{13}C CP transfers conditions at 10 and 40 kHz MAS rates for several CP schemes

We tested several approaches for polarization transfers under 10–40 kHz MAS rates (ω_{MAS}). One of them is the traditional ramped-CP (i.e., the linear gradient) with the 100 to 70% amplitude gradient applied on the ^{13}C channel, while employing a square pulse on deuterium. (Fig. 2A) [10,36]. The optimal transfer, defined as the maximum intensity at the M5- $^{13}\text{CD}_3$ site, was tested at $\omega_{\text{MAS}}/2\pi = 10$ kHz and yielded the

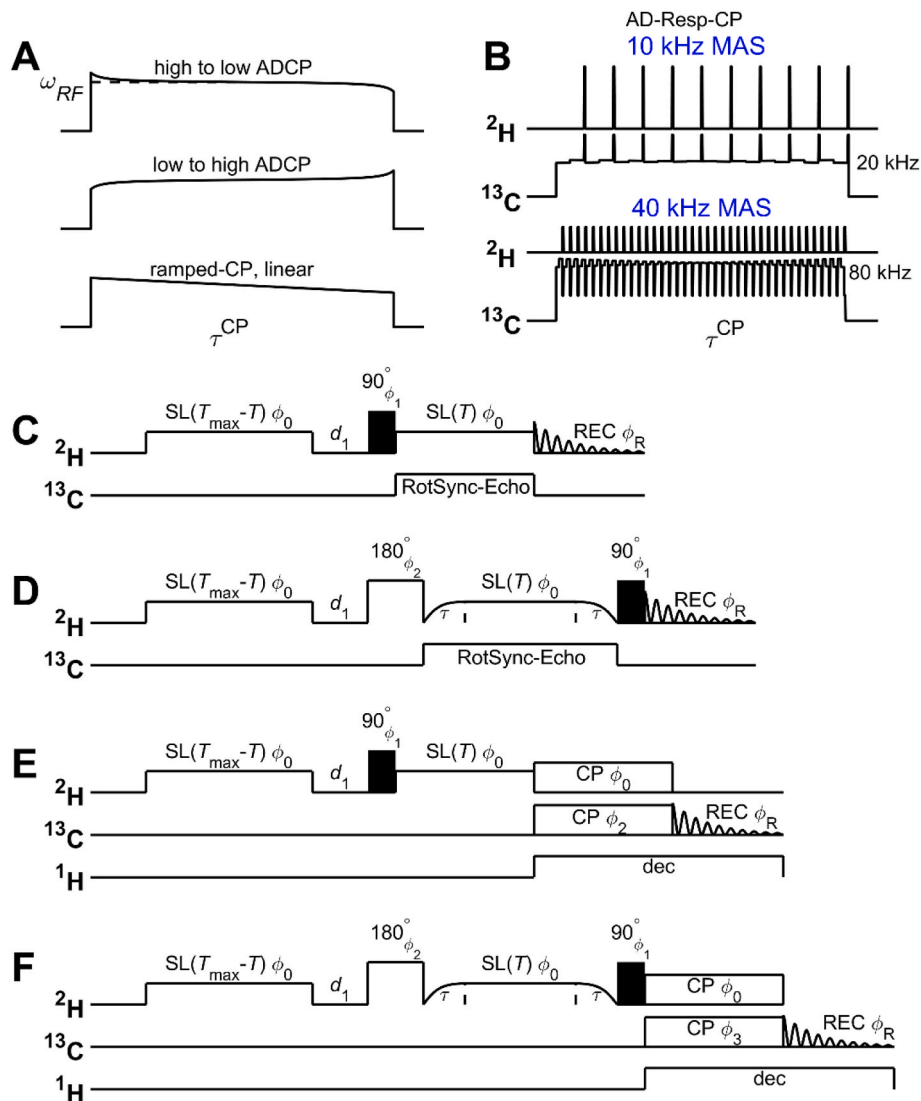


Fig. 2. A) The shapes of the CP pulses: the adiabatic versions of Eq. (1) corresponding to the high to low and low to high RF amplitude sweeps [37] and the ramped-CP with the gradient of 100 to 70%. B) The ^2H to ^{13}C AD-Resp-CP scheme at 10 kHz MAS and 40 kHz MAS rates [27]. The absolute vertical scales are chosen to display the relative scales for the two channels for each of the MAS rates. C) The ^2H $R_{1\rho}$ pulse sequence with ^2H -direct detection for the on-resonance case [21]. The heat compensation block $\text{SL}(T_{\max}-T)$ is followed by the inter-scan delay d_1 and the preparation 90° pulse, followed by a variable spin-lock delay (T), directly preceded by the FID collection. The phase cycle corresponds to $\phi_0 = x$, $\phi_1 = -y,y$, and the receiver = $-y,y$. An optional carbon decoupling period during the spin-lock time is displayed on the ^{13}C channel, which utilized the rotor-synchronized Hahn-echo sequence [35] with the phase modulation of (x,y,x,y,x,y,x,y,x) . D) The ^2H $R_{1\rho}$ pulse sequence for the off-resonance case with ^2H -direct detection [23], with the optional ^{13}C decoupling during the spin-lock period. Following the heat compensation and the inter-scan delay periods, an optional inversion pulse is preceded by the shaped pulse representing the variable spin-lock period (T), which is flanked on both sides by the adiabatic alignment ramp of the form \tanh/\tan . The phases are: $\phi_0 = x$, $\phi_1 = -y,y$, $\phi_2 = -x,-x$, and the receiver = $-y,y$. E) The incorporation of the ^2H to ^{13}C CP block into the ^2H $R_{1\rho}$ on-resonance case with ^{13}C detection. The CP block can include different scenarios of the linear ramp and tangential adiabatic sweep pulses, as well as AD-Resp-CP scheme, shown in A, B and described in the text. The phases are: $\phi_0 = x$, $\phi_1 = -y,y$, $\phi_2 = x,x,-x,-x,y,y,-y,-y$, and the receiver = $x,-x,-x,x,y,-y,-y,y$. Proton decoupling is applied during the CP and acquisition periods. F) The incorporation of the ^2H to ^{13}C CP block for the ^2H $R_{1\rho}$ off-resonance case, with the use of the optional inversion pulse preceding the magnetization alignment, as in D. The phases are: $\phi_0 = x$, $\phi_1 = -y,y$, $\phi_2 = x,x,-x,-x,y,y,-y,-y$, $\phi_3 = x,-x$ and the receiver = $x,-x,-x,x,y,-y,-y,y$.

following RF amplitudes: $\omega_{RF}^{13\text{C}}/2\pi = 47$ kHz for the carbon channel and $\omega_{RF}^{2\text{H}}/2\pi = 36.4$ kHz for the deuterium channel. For the amplitude-modulated pulses we specify the average amplitude during the shaped pulse. These amplitudes correspond to the first side-band matching condition, given by $\omega_{RF}^{13\text{C}} - \omega_{RF}^{2\text{H}} = \omega_{\text{MAS}}$. The optimized parameters are listed in Table 1 for 10 and 40 kHz MAS and the schemes' elements are shown in Fig. 2A and B.

We then proceeded to investigate different versions of the adiabatic sweep CP transfers (ADCP), with the RF amplitude modulation shape illustrated in Fig. 2A. The RF amplitude modulation of the CP pulse during this scheme follows the form of [37].

$$\omega_{RF}(t) = \omega_{RF} \mp b \tan(A(t/\tau^{CP} - 0.5)), \quad (1)$$

where ω_{RF} is the average value of the RF amplitude during the pulse, and τ^{CP} is the length of the pulse. The values of $A = \frac{14\pi}{15}$ (or 168°) and $b = \omega_{RF}/50$ were employed in our measurements [37]. The “-” sign corresponds to the sweep from high to low amplitude RF, while the “+” sign reverses the direction of the sweep. In general, these pulses can be applied either at a single channel (carbon-13 in our case) or both channels. There is no modulation of the phase.

During the application of the ADCP, we have found equivalent signal intensities for the two directions of the sweep, i.e., sweeping each of the

Table 1

Main experimental parameters used in all different CP schemes. The carriers were placed on resonance for both the ^{13}C and ^2H nuclei.

Scheme	τ^{CP} , ms		$\omega_{RF}^{13C}/2\pi$, kHz		$\omega_{RF}^{2H}/2\pi$, kHz	
	MAS	MAS	MAS	MAS	MAS	MAS
	10 kHz	40 kHz	10 kHz	40 kHz	10 kHz	40 kHz
ADCP, tangent both nuclei	3	2	42	55	31	24
ADCP, tangent on ^{13}C nuclei	3	2	42	55	31	24
AD-Resp-CP	1	1	19	78	35	35
ramped-CP (^{13}C)	1.5	Not tested	47		36.4	

channels from high to low or low to high amplitude directions. This applied to both the deuterium and carbon channels. The RF amplitudes yielding the maximum transfers (Table 1) are given by $\omega_{RF}^{13C} = 42$ kHz and $\omega_{RF}^{2H} = 31$ kHz at 10 kHz MAS, corresponding to the so-called zero-quantum CP matching condition [38]. At 40 kHz MAS, the optimized amplitudes yielded $\omega_{RF}^{13C} = 55$ kHz $\omega_{RF}^{2H} = 24$ kHz on ^2H , which corresponds to the so-called double-quantum CP matching condition, i.e. $2\omega_{MAS} = \omega_{RF}^{2H} + \omega_{RF}^{13C}$. The optimized contact time was found to be 3 ms for the 10 kHz MAS and 2 ms for the 40 kHz MAS rate. The RF amplitudes were calibrated using nutation measurements, with examples of nutation profiles shown in Fig. S2. During the CP and acquisition periods, proton decoupling using the SPINAL-64 scheme [39] was applied at 10 kHz MAS rate and the rotor-synchronized Hahn-echo decoupling scheme [35] at 40 kHz MAS rate, with the RF power for the proton 180° pulses of 80 kHz. We have verified that the ADCP scheme transfer efficiency is not significantly affected by the presence of proton decoupling, and the proton decoupling incorporation is likely not critical for the case of $S\text{-}^{13}\text{CD}_3$ system in the RC9 peptide. We also note that proton decoupling was employed during the $^2\text{H}\text{-}^{13}\text{C}$ CP transfer step in recent work by Shi et al. [1]

In an alternative deuterium to carbon-13 polarization transfer approach, the AD-Resp-CP scheme [27] was used, demonstrated in Fig. 2B. In this scheme, the adiabatic pulse with the average RF field amplitude of twice the MAS rate is applied to the carbon channel, while short rotor-synchronized pulses of equal RF strength are applied

simultaneously to both channels. The adiabatic modulation of the ^{13}C RF amplitude has an overall form of

$$\omega_{RF}(t) = 2\omega_{MAS} \mp b \tan(A(t/\tau^{CP} - 0.5)), \quad (2)$$

where $A = \frac{\pi}{2}$ (or 90°), $b = 6000 \text{ s}^{-1}$, and $\tau^{CP} = 1$ ms were used. We have rearranged the functional form of the amplitude modulation to emphasize its similarity with Eq. (1). In addition to the amplitude modulation, the ^{13}C channel undergoes phase modulations by reversing the phase every half of the rotor period. The rotor synchronized pulses on both channels were applied with $4 \mu\text{s}$ durations.

Experimentally, the optimized average RF amplitudes $\omega_{RF}^{13C} = 78$ kHz at 40 kHz MAS rate and $\omega_{RF}^{13C} = 19$ kHz RF at 10 kHz MAS rate, while the maximum ^2H RF amplitudes were 35 kHz at both MAS rates. The dependence of signal intensity on the ^2H power is weak, as found in the original publication [27]. This feature becomes important in the incorporation of the rotating frame relaxation period, as elaborated in the next section.

We show representative spectra obtained using these various CP schemes, as well as those using ^2H direct detection in Fig. 3. Additionally, the static spectrum of RC9 peptide obtained with the quadrupolar echo scheme [24] is shown (Fig. 3A, upper panel) to demonstrate the width of the powder pattern for the M5 -CD_3 group. Only the central band is visible for the ^{13}C spectra at all MAS rates (Fig. 3B), while for the ^2H spectra one observes the presence of side bands (Fig. 3A). At 10 kHz MAS rate the best transfer efficiency was obtained for the ADCP method utilizing the adiabatic ramps of Eq. (1) on both the ^2H and ^{13}C channels. The transfer efficiency was equivalent whether the amplitudes were swept from high to low or low to high directions. The transfer efficiency for the AD-Resp-CP scheme was somewhat lower in comparison to the double-tangent CP scheme, by the factor of about 1.5.

If only the ^{13}C amplitude is swept in the adiabatic fashion in the ADCP scheme, while the ^2H amplitude remains constant, the transfer efficiency is reduced compared to the case of sweeping the amplitudes on both channels, by the factor of 1.7. The results at 20 kHz MAS rates are analogous to those at 10 kHz MAS and are shown in Fig. S3. The worst transfer is obtained for the case of the ramped-CP with the linear gradient, with the reduction in the signal intensity by the factor of 3.4 compared with the best transfer given by the ADCP scheme. We have not

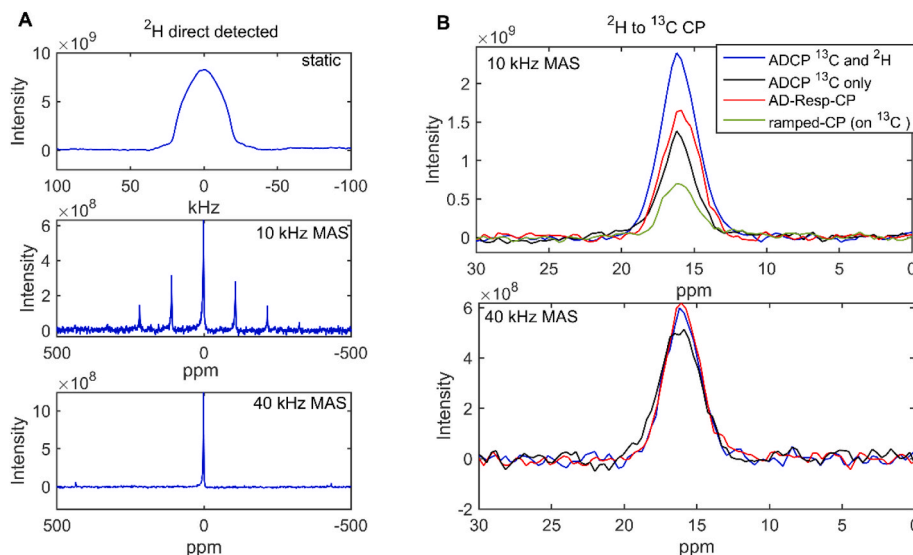


Fig. 3. Solid-state NMR spectra of the $\text{-}^{13}\text{CD}_3$ group of M5 in RC9 peptide. A) The ^2H -detected spectra under either static conditions or 10 and 40 kHz MAS rates, shown directly on the panels. The temperature set points were 300 K for the static conditions, 295 K for 10 kHz MAS rate, and 280 K for 40 kHz MAS rate. Other experimental parameters are listed in Table S1. B) The ^{13}C detected spectra at either 10 or 40 kHz MAS rates and at 14.1 T with different $^2\text{H}\text{-}^{13}\text{C}$ CP schemes, indicated directly on the panels and described in the text. The RF amplitudes and contact times are listed in Table 1. 512 scans and the line broadening function of 50 Hz were used. The ^{13}C spectra were referenced to the gamma polymorph of glycine [34].

tested the effect of the width of the ramp on the transfer efficiency, which, according to the results of Shi et al. [10] on the deuterated alanine, could impact the transfer efficiency significantly. The 70%–100% ramp on the ^{13}C nuclei used in our work corresponds to 14 kHz ramp width, while the optimal value could be different.

The AD-Resp-CP scheme was shown to be particularly effective for deuterons with larger values of the C_q constants, such as for example the C_α and C_β deuterons in proteins [1,12,27]. The relative transfer efficiencies for the single-channel AD-CP and the AD-Resp-CP at 10 and 20 kHz MAS (Fig. 3 and Fig. S3) are consistent with prior works [1,12,27]. The high efficiency of the adiabatic CP with the application of the tangent pulses on both channels for methyl groups is the new feature of this study.

At 40 kHz MAS the efficiencies of the transfers (Fig. 3B) are comparable for the ADCP scheme with the amplitude sweeps on both channels and the AD-Resp-CP scheme. If the adiabatic ramp is employed only on the ^{13}C channel, the efficiency is slightly reduced by the factor of 1.15. In general, the transfer efficiencies can be likely further improved by designing schemes that take into account RF inhomogeneities [40].

3.2. ^{13}C decoupling during the spin-lock period does not change the ^2H $R_{1\rho}$ rates

Before proceeding to the assessment of the incorporation of the cross-polarization schemes on the deuterium $R_{1\rho}$ rates, we need to confirm that the directly bonded carbon does not affect the relaxation rates for the case of the deuterium direct detection. This can be accomplished by comparing the rates with and without carbon decoupling during the spin-lock period. The pulse sequence for the measurements under the on-resonance and off-resonance ^2H spin-lock scenarios are illustrated in Fig. 2C and D. They utilize a heat compensation block and a variable length spin-lock period [21,23]. For the case of the off-resonance spin-lock [23], the deuterium magnetization is aligned with the use of the adiabatic ramps. The adiabatic alignment ramp has the modulations of the form $\omega_{RF}(t) = \omega_{RF} \frac{\tanh(\alpha t/\tau)}{\tanh \alpha}$, $\Delta\Omega(t) = \Delta\Omega_0 \frac{\tan(\beta[1-t/\tau])}{\beta}$ for the RF amplitude and the resonance frequency offset, respectively. The relevant parameters were set to: the sweep of $\Delta\Omega_0 = 120$ kHz, the pulse duration of $\tau = 200$ μs , and the steepness parameters $\alpha = 1.5$, $\beta = 5$ [23]. The optional inversion pulse before the alignment block increases the precision of the measurements.

Fig. 4 demonstrates $T_{1\rho}$ relaxation times obtained using the spin-lock field of $\omega_{SL}^{2H} = 25$ kHz with the on-resonance or several off-resonance

offset values. We compare the relaxation times in the absence of carbon decoupling to those obtained using carbon decoupling during the deuterium rotating frame relaxation period. The spin-lock RF amplitude of 25 kHz is sufficient at both MAS conditions for effective locking of the M5 methyl group of RC9 [21,22]. Its ^2H quadrupolar coupling constant (C_q) is about 30 kHz, based on the static powder pattern shown in Fig. 3A. An additional consideration for the ^2H spin-lock amplitude is that it needs to be chosen to avoid the rotary resonance conditions, given by $\omega_{SL}^{2H} = \frac{n}{2}\omega_{MAS}$, where n is an integer. When the value of $C_q > \omega_{MAS}/2\pi$ one can observe apparent shifts in these rotary resonance conditions from the above equation [21]. Fig. S4 shows simulations reflecting the expected quality of the spin-locking based on the interplay between the values of ω_{MAS} , ω_{SL}^{2H} , and C_q , Fig. S5 shows an example of the dependence of spin-locking efficiency as a function of C_q for $\omega_{MAS}/2\pi = 20$ kHz and $\omega_{SL}^{2H}/2\pi = 47$ kHz. The efficiency is significantly decreased for values of C_q above 70 kHz, reaching 66% for $C_q = 180$ kHz. A shifted very broad resonance is observed in the vicinity of $C_q = 115$ kHz, which is another manifestation of the effects of different crystallite orientations on the effective rotary resonance conditions under MAS for spin-1 nuclei.

The carbon decoupling was performed with the rotor synchronized spin-echo based method [35] using the RF value of the 180° pulses train of 55 kHz. The relaxation rates were obtained from fitting the magnetization decay curves (Fig. S6) to a mono-exponential function with the baseline: $M(t) = M_0 e^{-t/T_{1\rho}} + B$. For all tested scenarios, we did not observe any differences in the relaxation times with and without carbon decoupling, thus indicating that the presence of ^{13}C label does not affect ^2H rotating frame relaxation rates. This is likely due to the relatively weak ^{13}C - ^2H dipolar interaction, which can be further effectively removed by MAS.

3.3. Incorporation of the ADCP and AD-Resp-CP for indirect ^{13}C detection of ^2H $R_{1\rho}$ rates

We then proceed to the incorporation of the CP block into the ^2H rotating frame relaxation pulse sequences (Fig. 2 E, F), to enable detection on the carbon-13 nuclei. As our model compound has a single ^{13}C label, these pulse sequences represent a one-dimensional version, but can be modified for the incorporation of additional dimensions for application to multiply-labeled samples. In particular, ^{13}C - ^{13}C dipolar recoupling blocks [41] or the proton dimension for detection on protons [2,41,42] can be incorporated. We tested these pulse sequences for the two most efficient transfer schemes, the ADCP with the amplitude ramp

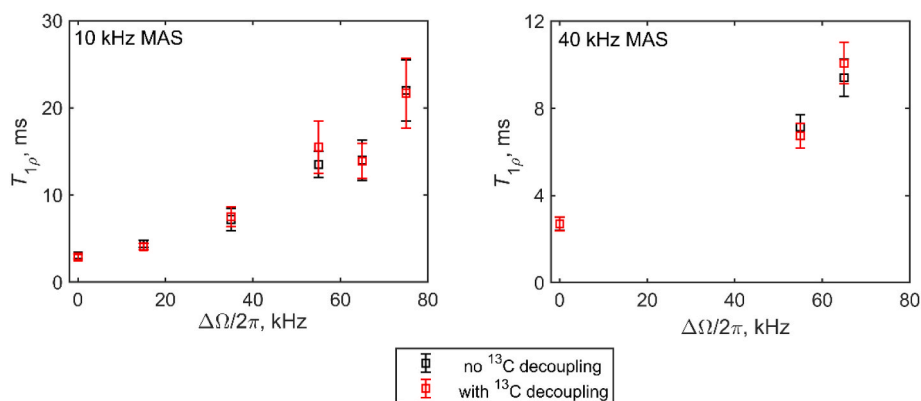


Fig. 4. ^2H $T_{1\rho}$ NMR relaxation times for the $^{-13}\text{CD}_3$ group of M5 in RC9 versus the values of the off-resonance offset $\Delta\Omega/2\pi$ obtained using the ^2H -direct detection pulses sequences of Fig. 2C and D with or without the optional carbon decoupling block, at 10 and 40 kHz MAS rates. The corresponding temperature set points were 295 and 280 K, respectively for the two MAS conditions, and the magnetic field is 14.1 T. The spin-locking field was 25 kHz and the ^{13}C decoupling utilized the spin-echo rotor-synchronized method [35] with the 55 kHz RF strength. The adiabatic ramps alignments for the ^2H magnetization in the off-resonance experiments [23] were performed with the \tanh/\tan pulse using the optimized adiabatic shape parameters specified in the text. The 90 and 180° ^2H pulses were at 75 kHz RF strength. The magnetization decay curves (Fig. S6) were constructed from the sum of intensities of the central band and the side-bands of the ^2H partially relaxed spectra and fitted to the mono-exponential function with the baseline.

sweeps on both channels and AD-Resp-CP. Our goal is to compare the relaxation times to the one obtained by ^2H direct detection, which facilitates a direct control of whether the CP transfer itself affects the relaxation rate. We start with the 10 kHz MAS rate condition and the ADCP scheme, using the pulse sequences of Fig. 2E.

When the ramp on deuterium is utilized with the sweep from higher to lower amplitude RF, with the resulting amplitude sweep is from 37 to 25 kHz when the average value is 31 kHz. A significant signal intensity loss is observed and the resulting $T_{1\rho}$ time is smaller in comparison to the ^2H direct detect method. The ^2H direct detect method yielded the relaxation time of 2.7 ± 0.4 ms with the spin-locking field of $\omega_{SL}^{2H} = 25$ kHz (Fig. S7), while the above approach yields 1.2 ± 0.4 ms. The intensity loss, measured using a very short relaxation period of 200 μs , is 50% compared to the intensity in the absence of the CP block. When the direction of the sweep on the ^2H channel is reversed from low to high (with the amplitude sweep from 25 to 37 kHz), we obtain the relaxation time of 2.2 ± 0.4 ms and recover 90–95% of the original intensity. The magnetization decay curve is shown in Fig. 5A. The direction of the sweep on the carbon channel does not influence the result. This implies that the jump in amplitudes from the ^2H spin-locking field value of 25 kHz to the value during the highest power of the CP amplitude ramp (37 kHz) disturbs the locked magnetization rather significantly. The best results in terms of accuracy and signal recovery are obtained when the CP sweep is implemented as a joint shape pulse with the spin-locking relaxation period and, in addition, when the RF amplitude of the spin-locking field during the relaxation period is as close to the RF amplitude at the beginning of the CP ramp as possible. We provide pulse program codes (using the Bruker Topspin programming syntax for the neo console) for the two versions of the pulse sequences, as well as the Matlab script example for generation of such a joint pulse in the SI1 and SI2.

Next, we evaluate the incorporation of the AD-Resp CP block under the 10 kHz MAS rate. The MATLAB script used to generate the AD-Resp-CP pulses is given in SI3. We first employ the CP block with the best matching condition in Table 1, corresponding to $\omega_{RF}^{2H}/2\pi = 35$ kHz, while the ^2H spin-lock RF amplitude during the relaxation period is 25 kHz. The resulting magnetization decay curve displays considerable oscillations, again suggesting that the magnetization behavior is not stable when the jump of the ^2H RF amplitude from 25 to 35 kHz is introduced (Fig. S7). We then take advantage of the fact that AD-Resp-CP transfer efficiency is rather insensitive to variations of the ^2H RF amplitude. In fact, less than 15% loss in signal intensity is observed when the AD-Resp-CP transfer is accomplished with the 25 kHz ^2H RF amplitude instead of the best match condition of 35 kHz. With this modification, the magnetization decay curve is well-behaved (Fig. 5A) and yields the relaxation time of 2.3 ± 0.5 ms, in comparison with the value of 2.7 ± 0.4 ms obtained with the ^2H direct detection. The results under 20 kHz MAS condition follow similar trends and examples are shown in Fig. S8. All measured values of ^2H $T_{1\rho}$ times are summarized in Table 2.

One of the likely factors leading to irregularities in the magnetization decay curves upon ^2H - ^{13}C transfers are interferences with the oscillating coherences orthogonal to the locked transverse coherence. In the presence of spin-lock and quadrupolar interactions, the initial transverse magnetization activates additional coherences from the set of eight spin-1 basis coherences [21,22,43]. They include the secular part of the quadrupolar coherence as well as one double quantum coherence. In the static case, the spin-locked coherence, defined as a state with zero eigenvalue for the Hamiltonian, includes the transverse magnetization and quadrupolar coherence. The coherences which include the double quantum term oscillate with the rate which depends both on the spin-lock field and the strength of the quadrupolar interaction. They tend to have slower relaxation rates, which are also dependent on

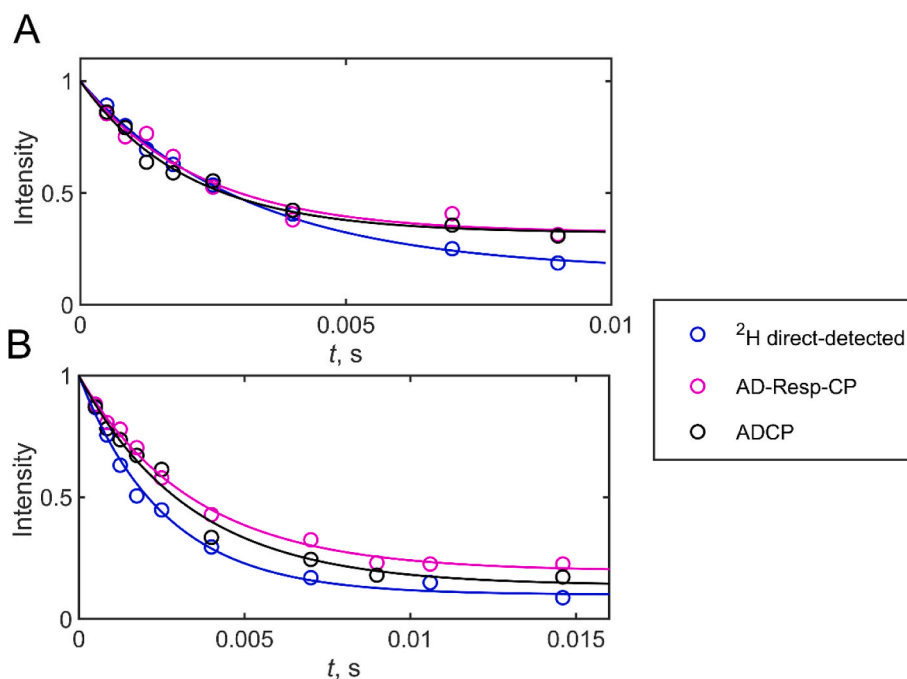


Fig. 5. Normalized magnetization decay curves for the on-resonance ^2H $T_{1\rho}$ measurements for the $^{-13}\text{CD}_3$ group of M5 in RC9, at 14.1 T and using spin-locking field strength of 25 kHz at 10 kHz MAS rate (A) or the spin-locking field of 27 kHz at 40 kHz MAS rate (B). Three approaches are shown: the two carbon-detected approaches with the use of pulse sequence of Fig. 2E and the ADCP scheme with the amplitude ramps on both channels given by Eq. (1) (black circles) or the AD-Resp-CP with the modulation on the ^{13}C channel given by Eq. (2) (magenta circles), as well as the ^2H direct detection approach, obtained with the pulse sequence in Fig. 2C (blue circles). For the ADCP scheme, the direction of the sweep on the ^2H channel is chosen for the best matching for the ^2H RF amplitudes during the ^2H $R_{1\rho}$ relaxation period and the starting point of the CP ramp. Additionally, the joint shaped pulse encompassing both the relaxation period and the CP pulse is encoded on the ^2H channel for the ADCP scheme. For the AD-Resp-CP scheme the RF power of the train pulses on the ^2H channel is chosen as close as possible to the RF amplitude of the spin-lock during the ^2H $R_{1\rho}$ relaxation period. Other experimental CP parameters are described in the text. The solid lines represent the fits performed using the monoexponential function with the baseline.

Table 2

Values of ${}^2\text{H}$ $T_{1\rho}$ times measurements for the $-^{13}\text{CD}_3$ group of M5 in RC9, at 14.1 T for different experimental schemes and conditions. Other parameters are specified in the text.

Schemes		${}^2\text{H}$ $T_{1\rho}$, ms		
		10 kHz MAS, 295 K	20 kHz MAS, 287 K	40 kHz MAS, 280 K
ADCP	matching ω_{RF}^{2H} and ω_{SL}^{2H} joint pulse	2.2 ± 0.4	2.2 ± 0.4	3.1 ± 0.4
	matching ω_{RF}^{2H} and ω_{SL}^{2H} not matching	2.7 ± 0.7		3.1 ± 0.5
	not matching ω_{RF}^{2H} and ω_{SL}^{2H}	1.2 ± 0.4	1.3 ± 0.2	
	not matching ω_{RF}^{2H} and ω_{SL}^{2H}	1.2 ± 0.4	1.3 ± 0.2	
RESP-CP	matching ω_{RF}^{2H} and ω_{SL}^{2H}	2.3 ± 0.5	2.6 ± 0.4	3.5 ± 0.4
	not matching ω_{RF}^{2H} and ω_{SL}^{2H}	4.5 ± 4		
	oscillations ω_{RF}^{2H} and ω_{SL}^{2H}			
${}^2\text{H}$ direct- detect		2.7 ± 0.4	2.4 ± 0.3	2.8 ± 0.4

crystallite orientations. Under MAS, the qualitative picture remains the same, but the precise composition of the locked and oscillating coherences must be determined by simulations. Further details are provided in SI4.

As the result, at the end of the variable spin-lock relaxation period their relative contribution can vary as a function of the relaxation delay (Fig. S9). The coherent oscillations lead to cancellation, due to averaging, of their contributions into the observable transverse magnetization in the direct-detect ${}^2\text{H}$ $T_{1\rho}$ measurements [22]. However, due to the imperfections of the CP transfers especially in the case of the abrupt change in the power of the ${}^2\text{H}$ RF field, they can lead to unwanted terms transferred to the ${}^{13}\text{C}$ nuclei via the dipolar coupling.

In addition to the on-resonance case, for the 10 kHz MAS rate we measured $T_{1\rho}$ relaxation times at the off-resonance conditions using the offset of $\Delta\Omega/2\pi = 35$ kHz and $\omega_{SL}^{2H}/2\pi = 25$ kHz, employing the pulse sequence of Fig. 2F. For the off-resonance case, the direction of the CP ramp sweep on the ${}^2\text{H}$ channel and exact matching of the ${}^2\text{H}$ channel RF powers of the spin-lock during the relaxation period and the CP block do not influence the stability of the magnetization decay curves, because the deuterium magnetization is brought back to the z-axis with the adiabatic alignment blocks prior to the CP period. For the fits of the magnetization decay curves (Fig. S10) we utilized the monoexponential function without the baseline in these cases, due to poorly defined baselines with our sampling times limited by the probe's duty cycle consideration in the presence of both the CP and spin-locking blocks. The maximum relaxation delay was 15 ms.

The measured values of the relaxation times are 11 ± 0.6 ms for the case of the ${}^2\text{H}$ direct method and 10.2 ± 1.0 ms for the case of the incorporation of the ADCP cross-polarization block. The results with the incorporation of the AD-Resp-CP block agree with the ${}^2\text{H}$ direct detection as well: 12.3 ± 1.0 ms with the monoexponential fit (Fig. S10). For the quantitative evaluation of the off-resonance $R_{1\rho}$ data in terms of modeling of the dynamics, it is important to obtain values of the longitudinal relaxation times, as they contribute to the relaxation in the tilted frame. We have, therefore, compared the ${}^2\text{H}$ T_1 values in the laboratory frame using the inversion recovery method either with the direct ${}^2\text{H}$ detection or with the incorporation of the respiration CP block. We found a good agreement in the ${}^2\text{H}$ T_1 values measured by the two techniques (Fig. S11): 272 ± 16 ms for the ${}^2\text{H}$ direct detection method, and 280 ± 30 ms for the AD-resp CP method with the 10 kHz MAS rate.

At the higher MAS of 40 kHz the spin-locking field during the relaxation period was applied on resonance using $\omega_{SL}^{2H} = 27$ kHz RF. Using the ADCP scheme with $\omega_{RF}^{2H}/2\pi = 24$ kHz, the resulting amplitude during the sweep from the high to low direction ranges from 28.8 to 19.2 kHz. This scenario can be applied without creating the jump in

powers from the relaxation to the CP periods and yield stable magnetization decay curves (Fig. 5B). The resulting $T_{1\rho}$ relaxation time of 3.1 ± 0.5 ms agrees within the precision of the measurement with the ${}^2\text{H}$ direct-detected value of 2.8 ± 0.4 ms. Using the AD-Resp-CP scheme and employing the $\omega_{RF}^{2H}/2\pi = 27$ kHz during the CP period to match the spin-locking field during the relaxation period, we obtain the $T_{1\rho}$ value of 3.5 ± 0.4 ms. With the use of $\omega_{RF}^{2H}/2\pi = 27$ kHz we found that the intensity loss from the best matching condition of $\omega_{RF}^{2H}/2\pi = 35$ kHz is minor, i.e., under 10%, in similarity to what we observed for the low MAS case.

In terms of extension to multiply labeled samples with additional carbon-13 (and, potentially, other nuclei) chemical evolution periods, it is important to note that it is advantageous to start the pulse sequences with the magnetization originating on deuterium. This permits for a shorter inter-scan delay due to much shorter deuterium T_1 relaxation times for methyl groups in proteins. ${}^2\text{H}$ T_1 times are often below 0.5 s in 310-280 K temperature range [3,5,10,12], in comparison to much longer ${}^{13}\text{C}$ T_1 relaxation times. The latter was found to be 21 ± 2 s for the ${}^{13}\text{C}$ methyl group at the M5 site of RC9, as measured at 40 kHz MAS at 280 K using the saturation recovery method. However, the relaxation rate itself should not depend on the order of the CP and the relaxation blocks.

For the potential applications to homogeneously deuterated proteins, one also needs to consider the effect of ${}^2\text{H}$ - ${}^2\text{H}$ spin diffusion [44], which needs to be tested experimentally. Spin diffusion is the distance-dependent magnetization transfer and can make the effective relaxation times more similar in different sites, especially under static conditions. However, the differences between the sites are retained to a substantial extent based on recent studies [10,45]. In particular, Figure 10 in Ref. [10] presents distinct ${}^2\text{H}$ T_1 relaxation times for individual sites in alanine, phenylalanine, and proline amino acids. Reference [45] expands the method to spider silk fibre, enriched with deuterated proline. The chemical shifts of the ${}^2\text{H}$ sites were determined to be very similar. Reference [44] emphasizes the effect of ${}^2\text{H}$ - ${}^2\text{H}$ spin diffusion for sites with similar chemical shifts.

Higher MAS rates may be advantageous for increasing the resolution and greatly suppressing the spin-diffusion effect, which is not expected to be a major factor. We note that relaxation due to quadrupolar interaction is less effective at higher MAS rates outside of the extreme narrowing limit, see Fig. 5 of reference [21]. Based on discussion in Ref. [43], further studies of the ${}^2\text{H}$ - ${}^2\text{H}$ spin diffusion effects under spin-locking conditions may be advantageous for quantitative interpretation of the relaxation rates. The potential minor spin diffusion effects under MAS can be further reduced by employing sparsely methyl-labeled samples, with spatially separated sites. Note that the relatively low spin-locking field under 35 kHz employed in this work will not be sufficient to lock most of the backbone sites, thus minimizing the potential effect of spin diffusion in the case of a fully deuterated side chain.

4. Conclusion

Using the RC9 peptide labeled at a single methyl group of M5, we have demonstrated that the ${}^2\text{H}$ - ${}^{13}\text{C}$ AD-Resp-CP and ADCP methods can be coupled with the ${}^2\text{H}$ rotating frame measurements for the detection on carbon nuclei. We tested both the on and off-resonance scenarios in the 10-40 kHz MAS rates range. This methodological step opens opportunities for extending the techniques for dynamics studies in multiply or sparsely labeled biomolecular systems. Special care must be taken in implementation of these techniques, in particular matching the RF powers of the deuterium spin-lock to the power at the beginning of the CP ramp in ADCP scheme, or to the power of the short ${}^2\text{H}$ pulses in the AD-Resp-CP scheme, as close as possible.

Declaration of competing interest

The authors declare that they have no known competing financial interests or personal relationships that could have appeared to influence the work reported in this paper.

Data availability

Data will be made available on request.

Acknowledgement

This work was supported by a National Institutes of Health Grant 1R15-GM111681. Part of the measurements were performed at the National High Magnetic Field Laboratory, which is supported by NSF Cooperative Agreement NSF/DMR-2128556, the State of Florida, and the U.S. Department of Energy. We thank Peter Gor'kov and Steve Ranner at NHMFL for their technical support with the NMR probe performance.

Appendix A. Supplementary data

Supplementary data to this article can be found online at <https://doi.org/10.1016/j.snmr.2024.101922>.

References

- [1] X. Shi, C.M. Rienstra, *J. Am. Chem. Soc.* 138 (2016) 4105–4119.
- [2] Ü. Akbey, *Solid State Nucl. Magn. Reson.* 125 (2023) 101861.
- [3] L. Vugmeyster, D. Ostrovsky, *Prog. Nucl. Magn. Reson. Spectrosc.* 101 (2017) 1–17.
- [4] R.R. Vold, Deuterium NMR studies of dynamics in solids and liquid crystals, in: R. Tycko (Ed.), *Nuclear Magnetic Resonance Probes of Molecular Dynamics*, Kluwer academic Publishers, Dordrecht, 1994, pp. 27–112.
- [5] S.M.D.C. Perera, X. Xu, T.R. Molugu, A.V. Struts, M.F. Brown, Solid-state deuterium NMR spectroscopy of rhodopsin, in: G.A. Webb (Ed.), *Modern Magnetic Resonance*, Springer International Publishing, Cham, 2018, pp. 1251–1270.
- [6] L.S. Batchelder, C.E. Sullivan, L.W. Jelinski, D.A. Torchia, *Proc. Natl. Acad. Sci. U. S.A.* 79 (1982) 386–389.
- [7] H.E. Ferreira, G.P. Drobny, *Biointerphases* 12 (2017) 02D418.
- [8] K. Li, P.S. Emani, J. Ash, M. Groves, G.P. Drobny, *J. Am. Chem. Soc.* 136 (2014) 11402–11411.
- [9] L. Vugmeyster, *Solid State Nucl. Magn. Reson.* 111 (2021) 101710.
- [10] X. Shi, J.L. Yarger, G.P. Holland, *J. Magn. Reson.* 226 (2013) 1–12.
- [11] U. Akbey, A.J. Nieuwkoop, S. Wegner, A. Voreck, B. Kunert, P. Bandara, F. Engelke, N.C. Nielsen, H. Oschkinat, *Angew. Chem.* 53 (2014) 2438–2442.
- [12] Ü. Akbey, *J. Magn. Reson.* 327 (2021) 106974.
- [13] M.D. Geleiter, K.J. Chen, M. Hong, *J. Biomol. NMR* 75 (2021) 335–345.
- [14] D.D. Boehr, R. Nussinov, P.E. Wright, *Nat. Chem. Biol.* 5 (2009) 789–796.
- [15] P. Schanda, M. Ernst, *Prog. Nucl. Magn. Reson. Spectrosc.* 96 (2016) 1–46.
- [16] A.G. Palmer 3rd, *J. Magn. Reson.* 241 (2014) 3–17.
- [17] P. Rovó, *Solid State Nucl. Magn. Reson.* (2020) 101665.
- [18] C. Quinn, A. McDermott, *J. Biomol. NMR* 45 (2009) 5–8.
- [19] A. Krushelnitsky, D. Gauto, D.C. Rodríguez Camargo, P. Schanda, K. Saalwachter, *J. Biomol. NMR* 71 (2018) 53–67.
- [20] P. Schanda, *J. Magn. Reson.* 306 (2019) 180–186.
- [21] L. Vugmeyster, D. Ostrovsky, A. Greenwood, R. Fu, *J. Magn. Reson.* 337 (2022) 107171.
- [22] L. Vugmeyster, D. Ostrovsky, *ChemPhysChem* 20 (2019) 333–342.
- [23] L. Vugmeyster, A. Rodgers, D. Ostrovsky, C. James McKnight, R. Fu, *J. Magn. Reson.* 352 (2023) 107493.
- [24] R.L. Vold, R.R. Vold, Deuterium relaxation in molecular solids, in: W. Warren (Ed.), *Advances in Magnetic and Optical Resonance*, Academic Press, San Diego, 1991, pp. 85–171.
- [25] D. Marks, N. Zumbulyadis, S. Vega, *J. Magn. Reson.* 122 (1996) 16–36.
- [26] P. Hodgkinson, C. Auger, L. Emsley, *J. Chem. Phys.* 109 (1998) 1873–1884.
- [27] S.K. Jain, A.B. Nielsen, M. Hiller, L. Handel, M. Ernst, H. Oschkinat, U. Akbey, N. C. Nielsen, *Phys. Chem. Chem. Phys.* 16 (2014) 2827–2830.
- [28] M. Hologne, K. Faelber, A. Diehl, B. Reif, *J. Am. Chem. Soc.* 127 (2005) 11208–11209.
- [29] M. Hologne, Z. Chen, B. Reif, *J. Magn. Reson.* 179 (2006) 20–28.
- [30] D. Wei, Ü. Akbey, B. Paaske, H. Oschkinat, B. Reif, M. Bjerring, N.C. Nielsen, *J. Phys. Chem. Lett.* 2 (2011) 1289–1294.
- [31] L. Vugmeyster, A. Rodgers, K. Gwin, D. Ostrovsky, S.L. Smirnov, *bioRxiv* (2023), <https://doi.org/10.1101/2023.02.16.528870>.
- [32] L. Vugmeyster, D. Ostrovsky, A. Rodgers, K. Gwin, S.L. Smirnov, C.J. McKnight, R. Fu, *ChemPhysChem* (2023), <https://doi.org/10.1002/cphc.202300565>.
- [33] G.L. Butterfoss, E.F. DeRose, S.A. Gabel, L. Perera, J.M. Krahn, G.A. Mueller, X. Zheng, R.E. London, *J. Biomol. NMR* 48 (2010) 31–47.
- [34] M.J. Potrzebowski, P. Tekely, Y. Dusaouy, *Solid State Nucl. Magn. Reson.* 11 (1998) 253–257.
- [35] X. Filip, C. Tripon, C. Filip, *J. Magn. Reson.* 176 (2005) 239–243.
- [36] G. Metz, X.L. Wu, S.O. Smith, *J. Magn. Reson.* 110 (1994) 219–227.
- [37] Y. Li, S. Zhang, Z. Wu, X. Peng, R. Fu, *Magn. Reson. Lett.* 2 (2022) 147–158.
- [38] M.J. Duer, *Solid-State NMR Spectroscopy*, Blackwell Publishing Ltd, Oxford, 2004.
- [39] T. Bräuniger, P. Wormald, P. Hodgkinson, *Monatsh. Chem.* 133 (2002) 1549–1554.
- [40] A. Šmelko, J. Blahut, B. Reif, Z. Tošner, *Magnes. Res.* 4 (2023) 199–215.
- [41] D. Mance, M. Weingarth, M. Baldus, Solid-state NMR on complex biomolecules: methods and applications, in: G.A. Webb (Ed.), *Modern Magnetic Resonance*, Springer International Publishing, Cham, 2018, pp. 487–503.
- [42] D.H. Zhou, G. Shah, M. Cormos, C. Mullen, D. Sandoz, C.M. Rienstra, *J. Am. Chem. Soc.* 129 (2007) 11791–11801.
- [43] J.R.C. van der Maarel, *J. Chem. Phys.* 99 5646–5653.
- [44] B. Reif, Y. Xue, V. Agarwal, M.S. Pavlova, M. Hologne, A. Diehl, Y.E. Ryabov, N. R. Skrynnikov, *J. Am. Chem. Soc.* 128 (2006) 12354–12355.
- [45] X. Shi, J.L. Yarger, G.P. Holland, *Chem. Commun.* 50 (2014) 4856–4859.